COBEM 2021 26th International Congress of Mechanical Engineering
November 22-26, 2021, Virtual Congress, Brazil

COB-2021-0856
EXPLORATORY INVESTIGATION ON RESIDUAL STRESS AND DISTORTION OF 20MnCr5 CARBURIZING STEEL PROCESSED BY LASER POWDER BED FUSION

Lucas Robatto
Ronnie Rego
Anderson Borille
Aeronautics Institute of Technology - ITA, Competence Center in Manufacturing - CCM. Praça Marechal Eduardo Gomes, 50, Vila das Acácias. CEP 12.228-900. São José dos Campos, SP, Brazil.
robatto@ita.br, ronnie@ita.br, borille@ita.br

José Mascheroni
Arthur Kretzer
Alkimat Tecnologia. Rua Aberlardo Manoel Peixer, 142, Barreiros. CEP 88.110-055. São José, SC, Brazil.
jose@alkimat.com.br, arthur.kretzer@alkimat.com.br

Abstract. *New demands of the automotive transmission industry require solutions that the additive manufacturing technique of laser powder bed fusion (L-PBF) presents potential to provide. However, knowledge on the surface integrity induced by the L-PBF process is still incipient for residual stress (RS) and distortion control for transmission applications, important aspects for proper fatigue resistance and dimensional quality assurance. In this work, an exploratory investigation on the RS and distortion dependence on the hatch spacing and laser power of L-PBF with 20MnCr5 carburizing steel was conducted. RS and topography maps of L-PBF specimens processed with different parameters were obtained through X-ray diffractometry and profilometry, respectively. Larger hatch spacing was related to reduced residual stress heterogeneity and lower distortion effects, but higher FWHM of the diffraction profiles. The findings contribute for the technological maturity of L-PBF introducing new aspects to be considered in parameters optimization.*

Keywords: *Additive manufacturing, X-ray diffraction, topography, heterogeneity, gears*

1. INTRODUCTION

In the context of Industry 4.0 and electromobility, challenging demands in several areas have been emerging for the automotive sector, especially in terms of product and manufacturing. The transmission of electric vehicles, for instance, presents stricter requirements of noise and vibration, efficiency and fatigue resistance (Rodrigues, 2018; Robatto, 2021). The traditional processes for gear manufacturing based on machining, however, are in the limit of their capability and have evolved incrementally in the last years. One of the technologies of Industry 4.0 which is considered to have potential of disruptiveness for facing the mentioned changes of requirements is Additive Manufacturing (AM). AM consists of a group of processes in which parts are produced layer-by-layer from a digital model (ISO 52900). Due to its layerwise principle, AM can expand possibilities of product design freedom, materials and performance (Gibson *et al.*, 2010).

One of the most common metal AM techniques is Laser Powder Bed Fusion (L-PBF). The principle of the L-PBF process is the use of laser to selectively melt layers of powder over a bed. This principle of localized heat input induces surface integrity states that differ from those induced by conventional processes, resulting in heterogeneous properties (Barlett and Li, 2019). For the application of metal AM for parts which require high mechanical resistance, such as automotive transmission gears, this knowledge on surface integrity is essential, since it is directly linked to the part's performance (Hauk, 1997).

The literature that covers the surface integrity aspects of microstructure, residual stress (RS) and topography of additively manufactured carburizing steels for gear applications is up to the present moment limited. Schmitt *et al.* (2020) described the mechanical and material properties of L-PBF processed 16MnCr5, but a fundamental analysis of the process influences on the surface integrity was not covered. Kluge (2017) found high scatter in the fatigue life of AM gears made of 20MnCr5 steel, but the reasons for this were not discussed, which could be related to surface integrity heterogeneity, as described by Rego (2016).

The relationship between L-PBF parameters, RS and the consequent distortions of carburizing steels is a topic still underexplored by the scientific community. The objective of the present study is to provide an exploratory assessment of how RS and distortions can be influenced by L-PBF parameters on the processing of a 20MnCr5 gear carburizing steel.

RS mappings and topography analyses of L-PBF specimens with different laser powers and hatch spacings are performed for such purpose.

2. MATERIALS AND METHODS

The hypothesis to be proven in this study was that the variation of a selected range of L-PBF parameters influences RS intensities, heterogeneity and distortions of parts of carburizing steels. The L-PBF process was performed in an Alkimat Laser Funde200 machine equipped with a fiber laser. The material of the fabrications was a 20MnCr5 steel (DIN 10084:2008-06) spherical powder with a mean size of 29.5 µm and volume based distribution parameters D_{10} 19.9 µm, D_{50} 32.2 µm and D_{90} 43.3 µm, obtained through Dynamic Image Analysis. The process was conducted in an inert nitrogen atmosphere, generally used for Fe-based alloys to prevent the material from intense oxidation and to enable the removal of process by-products. The geometry of the specimens was a 10x10x2 mm prism. The experimental plan consisted on the analysis of six combinations of L-PBF parameters, in which three laser power values of 165, 170 and 185 W and two hatch spacings values of 100 and 140 µm were selected.

A layer thickness of 30 µm and a scanning speed of 550 mm/s were fixed parameters. The infill scan strategy of choice consisted of a meander pattern with bidirectional scan. A 67° of rotation between each layer was adopted, because the rotation leads to remelting of pore areas between tracks of previous layers and the prime number 67 ensures that the scan vector does not repeat, which increases the homogeneity of microstructure. A single track contour was produced before the infill and with the same parameters of each treatment. After manufacturing, the specimens were removed from the baseplate by sawing and were analyzed in the as-built state. The L-PBF experiments conditions are illustrated in Figure 1 and the specimens' nomenclatures and corresponding parameters are listed in Table 1.

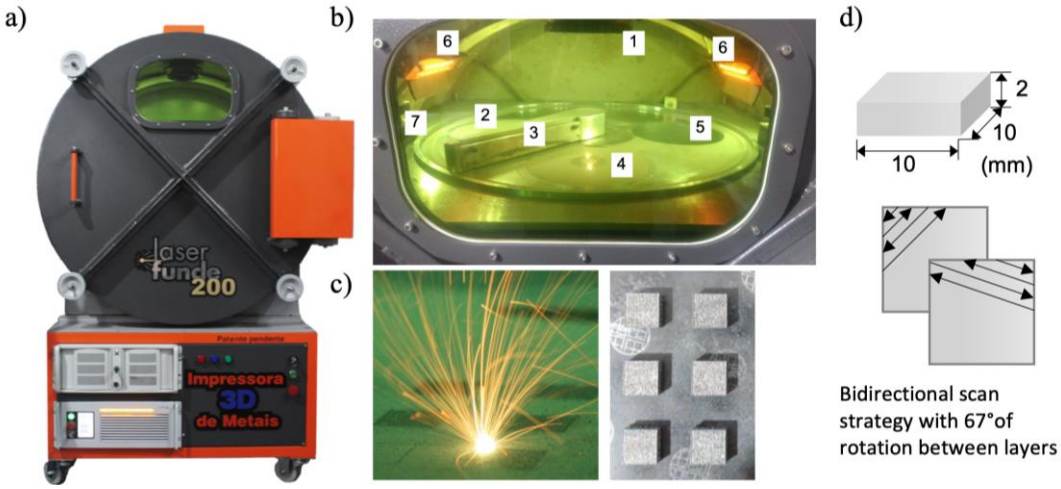

Figure 1. a) Alkimat Laser Funde200 L-PBF machine in which the specimens manufacturing was conducted. b) 1: laser system, 2: feeding chamber, 3: recoater, 4: manufacturing chamber, 5: chamber for powder overflow, 6: infrared heaters, 7: inert gas outlet. c) specimens manufacturing, d) specimens' geometry and scan strategy.

Table 1. L-PBF parameters of the specimens.

Specimen	Laser Power (W)	Hatching spacing (µm)
P165-H140	165	140
P170-H140	170	140
P185-H140	185	140
P165-H100	165	100
P170-H100	170	100
P185-H100	185	100

The specimens were mapped in terms of RS distribution through X-ray diffractometry with a Pulstec diffractometer µ-X360n after removal from the L-PBF baseplate. The analyzed diffraction angle was the 156° of the Cr-$K_{\alpha 1}$ radiation for ferritic and martensitic steels (ASTM E2860-12) and the method of measurement was the cosα described by Tanaka (2019). The measurement spot had a diameter of 2 mm and four points at the corners of the top surface were measured in two directions: parallel (RSy – y direction) and perpendicular to the scan tracks (RSx – x direction). The influences of the L-PBF laser power and hatch spacing on the macro RS and the full width at half maximum (FWHM) of the diffraction

peaks were investigated. FWHM represents combined effects of crystallite size and microstrains (Hauk, 1997), which can be an indication of RS heterogeneity (Rego, 2016). Figure 2 shows a schematic of the RS measurements.

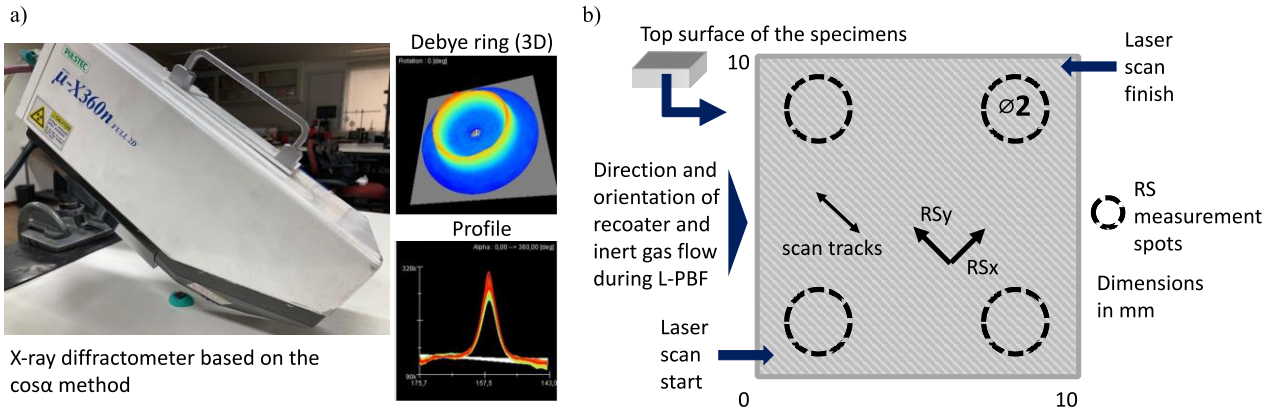

Figure 2. a) Residual stress measurements through the cosα method. b) positions and directions of RS mappings over the top surface of the specimens.

The topography analysis was based on distortion investigations over the specimens` top surface with a Taylor Robson Surtronic S-130 rugosimeter. Ten profiles of 9.6 mm parallel to one of the edges were merged tridimensionally and had the roughness filtered. The heights variation range and distributions were then analyzed according to the influence of the L-PBF process and compared with the measured RS. Figure 3 illustrates the topography analyses.

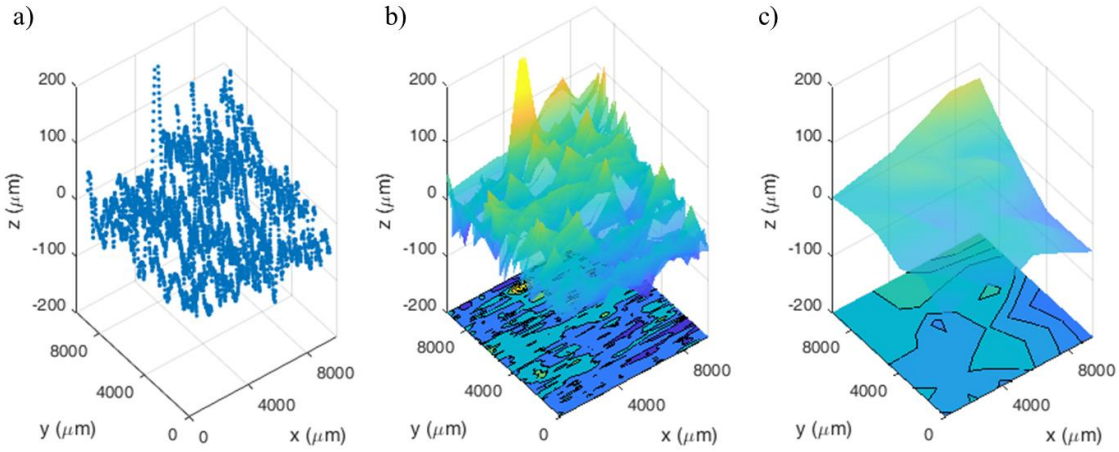

Figure 3. a) Topography point cloud. b) Surface and contour map. c) Roughness filtering.

To verify if the RS and topography results are a direct consequence of internal porosity induced by the different L-PBF parameters, the specimens had their relative density calculated through the Archimedes principle (ASTM B311-17), with an analytical balance of 0.0001 g resolution, according to Eq. (1). Each specimen was measured 5 times in the dry and wet states and the measurement uncertainty was calculated considering the propagation of errors and a 95% confidence level.

$$\rho_{relative} = \left(\frac{m_{air}}{m_{air} - m_{distilled\ water}}\right) \frac{\rho_{distilled\ water}}{\rho_{wrought\ 20MnCr5}} \tag{1}$$

in which $\rho_{relative}$ is the relative density of the specimen, m_{air} is its mass measured in air, $m_{distilled\ water}$ is it mass measured in distilled water, $\rho_{distilled\ water}$ is the density of the distilled water at the given temperature and $\rho_{wrought\ 20MnCr5}$ is the density of the material 20MnCr5 conventionally processed with zero porosity, which is 7850 g/m^3 (Ranganathan *et al.*, 2019).

3. RESULTS AND DISCUSSION

According to Figure 4, the relative densities of the specimens were between 94% and 100%, considering a 95% confidence level. Through the error bars, it can be perceived that the L-PBF parameters selected did not generate significant differences in the specimens' density. Therefore, for the subsequent analysis of RS and topography, the differences found were not attributed to porosity hypotheses.

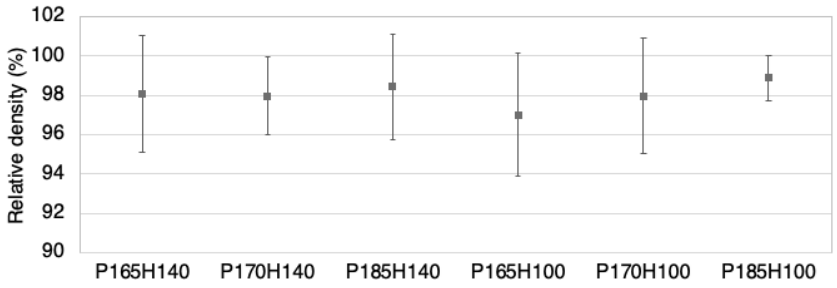

Figure 4. Relative densities of the L-PBF specimens. Error bars representing a 95% confidence level.

Figure 5 shows the average RS of the top surfaces of the specimens with 95% confidence level uncertainties. The conditions were not significantly different and the results were characterized by large dispersion, both in terms of RSx and RSy. This indicated that the RS distribution on the samples is highly heterogeneous, which motivated the construction of RS maps according to different regions of the specimens. It could be observed that the RS in the direction perpendicular to the scan tracks, RSx, present lower intensities than the RSy parallel to the scan tracks. The same observation is generally valid for welding processes, which present similarities with L-PBF (Oliveira et al., 2020). The RS in the direction perpendicular to weld tracks is normally lower than in the parallel direction, due to less restrictions of melt pool shrinkage during cooling. In case of low heat inputs, compressive RS in the transverse direction of welds can also be compressive (Zinn and Scholtes, 2002). The same mechanism explains the L-PBF RS results obtained.

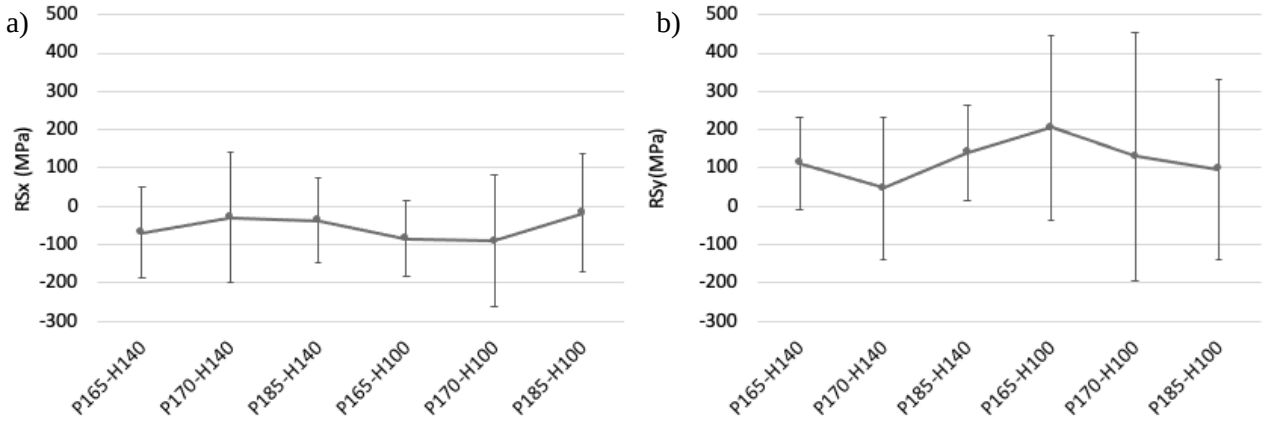

Figure 5. Average results of residual stress at the top surfaces of the L-PBF specimens. a) RSx, residual stress in the direction perpendicular to scan tracks. b) RSy, residual stress in the direction parallel to scan tracks.

The RS maps of the top surfaces of the specimens are then presented in Figure 6. The RS anisotropy between the x- and y-directions as a result of the L-PBF process (Barlet and Li, 2019) was still observed after the specimens removal from the baseplate, which indicates that the RS at the top surface of the specimen was preserved. For all the specimens, compressive RS values were found in the x-direction perpendicular to the L-PBF tracks, while tensile values corresponded to the y-direction parallel to the tracks. While the RS differences between the x- and y-directions for each condition was evident, the major differences between the specimens can be observed for RSy. The specimens with hatch spacing of 100 μm presented higher levels of RSy heterogeneity, which means they are more prone to distortion when subjected to further RS relaxation effects and to reduced fatigue resistance (Rego, 2016). The specimens produced with 140 μm of hatch spacing presented the lowest RS heterogeneities. Higher hatch spacings are related to lower energy densities, which have been associated in the literature to less intense RS (Barlet and Li, 2019). However, the RS heterogeneity dependence on the hatch spacing have not yet been described. This can be attributed to reduced shrinkage impeding mechanisms for tracks with higher hatchings, which reduces the effects of one track over another in L-PBF multi-tracks and multilayers.

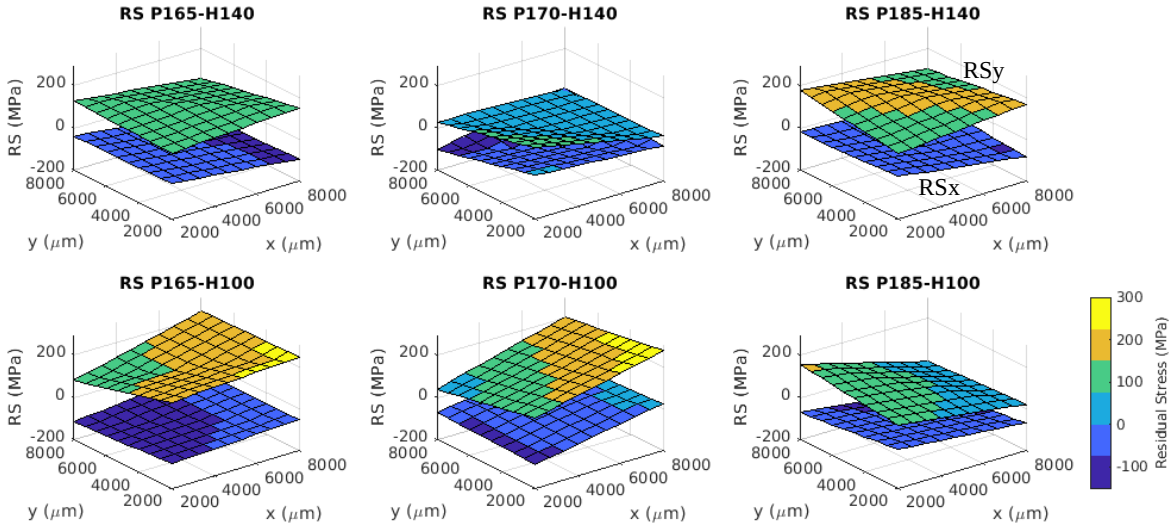

Figure 6. RS maps of the for L-PBF specimens.

The FWHM data shown in Figure 7 obtained from the diffraction mapping presented shorter dispersion between the corners of the specimens, no apparent x-y anisotropy and an indication of the response dependency on the L-PBF parameters. Lower hatch spacing induced higher FWHM values with statistical significance, as shown in Figure 7(b). As FHWM represents the diffraction peak broadening, lower hatch spacings can be associated to increased heterogeneity in the microscale in terms of crystallite size and microstrain (Hauk, 1997). Therefore, the L-PBF conditions can present different effects of RS heterogeneity in the macro- and micro scales, which deserve further investigations, since both play an important role in fatigue behavior (Scholtes, 2000). Further diffraction peak deconvolution methods and surface integrity assessment should then be employed to identify the reasons for the FWHM differences in terms of crystallite size and microstrain, according to Hauk (1997). The fact that FWHM presented a low dispersion over the four corners of the top surfaces of the specimens also suggests that FWHM is less susceptible to variation after baseplate removal than the macro RS, which is in accordance with the localized and average coverage of each response, respectively.

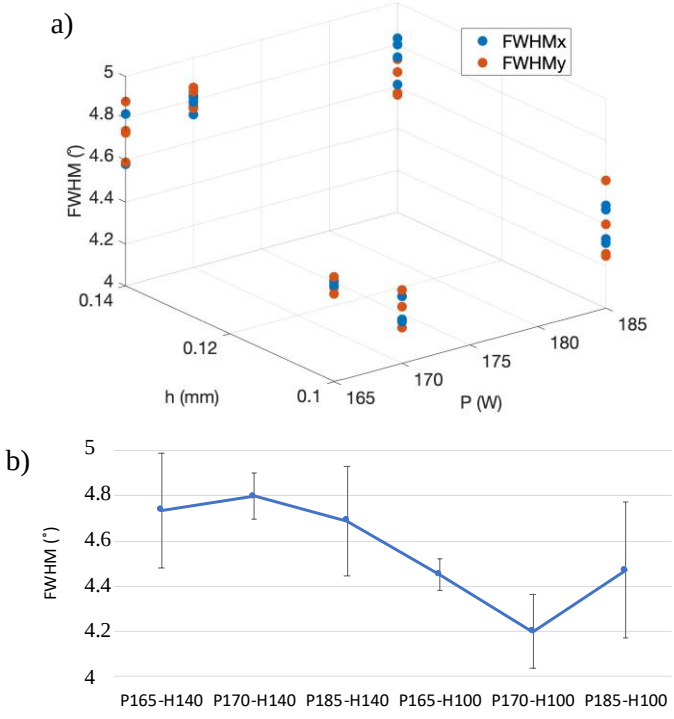

Figure 7. FWHM plotted according to laser power and hatch spacing. a) FWHM from x- and y- diffraction measurements. b) Statistical comparison between the specimens.

The topography of the top surfaces after roughness filtering are exhibited in Figure 8. It can be observed that the extremities near X = Y = 10000 μm presented higher heights, while regions near X = Y = 0 μm presented depressions for most specimens. This similarity is in accordance with the equal scanning strategy and angle of rotation between layers. The depression coincided with the corner where the laser scanning began at the top layer, and the protuberance coincided with corner where it finished. Some differences between the conditions however can be observed in terms of heights variation range, as shown in Table 2.

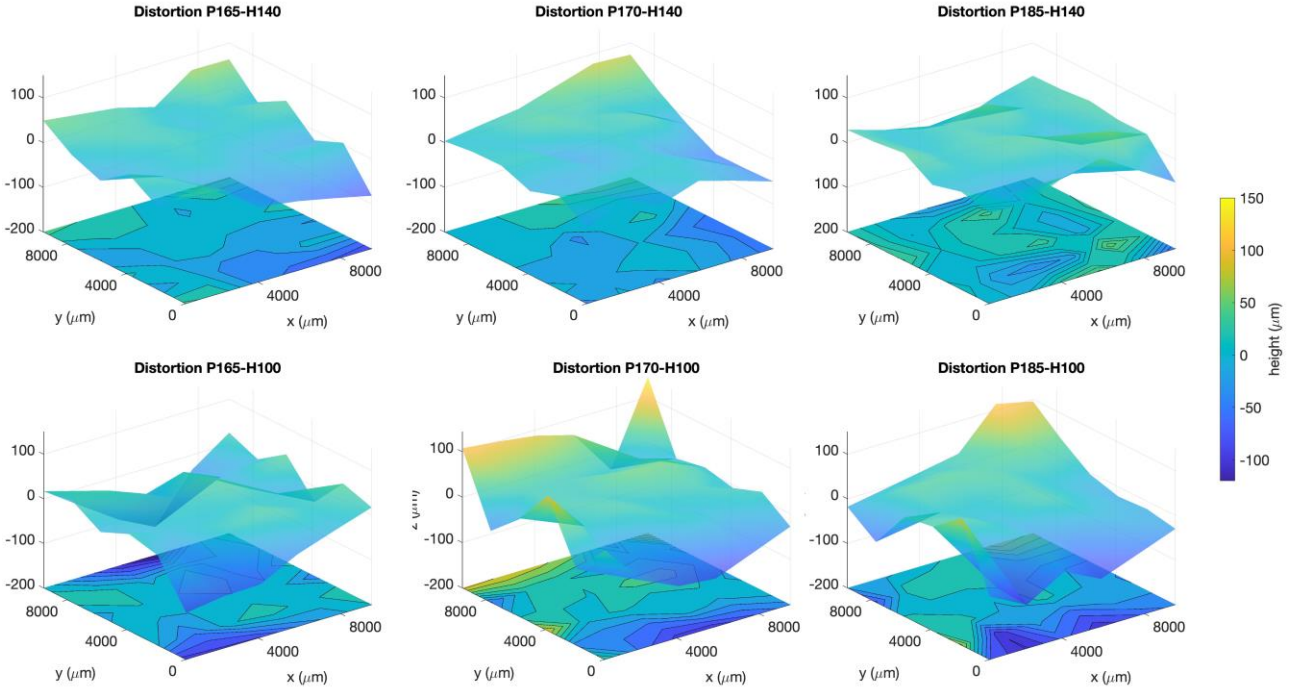

Figure 8. Surface plot of the top surface of the specimens after roughness filter.

Table 2. Heights variation ranges.

Specimen	Δh (μm)
P165-H140	146
P170-H140	131
P185-H140	109
P165-H100	178
P170-H100	238
P185-H100	216

The specimens of hatch spacing 140 μm presented the lowest heights variation range and also the lowest macro RS heterogeneities. This suggests that higher hatch spacings may reduce the effects of RS and distortions, which may be a favorable approach for the improvement of surface integrity of transmission components. However, increasing the hatch spacing may also have a detrimental effect of increasing the susceptibility to L-PBF process porosity, as described in other studies (Plessis, 2019). Such relations reinforce the complexity of the L-PBF variables on the surface integrity features, characterized by trade-offs between positive and negative effects. For the specimens with h = 100 μm the higher heights variation range were associated with the more heterogeneous RS prior discussed.

4. CONCLUSION

In this work RS distributions and distortion analyses with L-PBF specimens of carburizing steel 20MnCr5 with different laser power and hatch spacing were performed. The following conclusions can be drawn:

- The RSy, in the direction parallel to the L-PBF tracks, presented higher intensities and heterogeneity than the RSx perpendicular to the tracks.
- Higher hatch spacings induced less heterogeneous RS.

- The FWHM of the diffraction peaks increased with hatch spacing. Therefore, different RS heterogeneities responses in the macro- and microscales were found.
- An indicative of association between macro RS heterogeneity and distortion could be observed and the hatch spacing induced the major differences in such responses. Increasing hatch spacing can reduce macro RS heterogeneity and distortion effects.
- The findings introduce new aspects to be considered for L-PBF parameters optimization and provide knowledge for the control of RS of L-PBF components for automotive transmission applications. Extending the analyses to other L-PBF parameters in wider ranges and to other surface integrity responses are part of an ongoing research for such purpose.

5. ACKNOWLEDGEMENTS

This study was financed in part by the Coordenação de Aperfeiçoamento de Pessoal de Nível Superior - Brasil (CAPES) - Finance Code 001, and by the companies Gerdau and Braskem. The authors acknowledge the support of VAS Tecnologia Industrial with the X-ray Diffractometry experiments and the students Izabel Criscuolo and Gabriel Patrocínio for the support with topography measurements.

6. REFERENCES

ASTM B311 – 93, 2002. “Standard Test Method for Density Determination for Powder metallurgy (P/M) Materials Containing Less than Two Percent Porosity”, American Society for Testing and Materials.

ASTM E2860-12, 2012. “Standard method for residual stress measurement by X-ray diffraction for bearing steels”. American Society for Testing and Materials.

Barlett, J.L. and Xiaodong, l., 2019. “An overview of residual stresses in metal powder bed Fusion”. Additive manufacturing, Vol. 27, pp. 131-149.

DIN EN 10084 2008-06, 2008. “Case hardening steels – Technical delivery conditions”. European Committee for Standardization.

Gibson, I., Rosen, D. and Stucker, B., 2015. “Additive manufacturing technologies”. Springer, Second Edition.

Hauk, V., 1997. “Structural and residual stress analysis by nondestructive methods”. Elsevier.

ISO/ASTM 52900:2015, 2015. “Additive Manufacturing - General Principles – Terminology”. International Standard Organizaton, pp. 1-19.

Kluge, M., Kotthof, G., Cavallini, C. and Höges, S., 2017. “Design and production of innovative transmission components with additive manufacturing”. In Proceedings of the 16th International CTI Symposium Automotive Transmissions, HEV and EV drives. Berlin, Germany.

Oliveira, J.P., Santos, T.G., Miranda, R.M., 2020. “Revisiting fundamental welding concepts to improve additive manufacturing: From theory to practice”. Progress in Materials Science, Vol. 107.

Plessis, A., 2019. “Effects of process parameters on porosity in laser powder bed fusion revealed by X-ray tomography”. Additive Manufacturing, Vol. 30.

Ranganathan, S., Prakash, J., Mathew, D., 2019. Appraisal of Tribo Meter Study on 20MnCr5 Alloy Steel under Case Hardened and Shot Peened Condition. SAE International.

Rego, R., 2016. “Residual Stress interaction in-between processes of the gear manufacturing Chain”. Doctorate Thesis. Aeronautics Institute of Technology, São José dos Campos, Brazil.

Robatto, L. and Rego, R., 2021 “Engrenagens 4.0: As Superengrenagens na Indústria Automotiva do Futuro”. Engrenagens: Gear Magazine, Vol. 4, pp. 33-36.

Rodrigues, C.D.P., 2018. “Design of a high-speed transmission for an electric vehicle”. Master’s Dissertation. Universidade do Porto. Porto, Portugal.

Tanaka, K., 2019. “The cosα method for x-ray residual stress measurement using two-dimensional Detector”. Mech. Eng. Rev., Vol. 6(1), pp. 1-15.

Schmitt, M., Kamps, T., Sigmüller, F., Winkler, J., Schlick, G., Seidel, C., Tobie, T., Stahl, K. and Reinhart, G., 2020. “Laser-based powder bed fusion of 16MnCr5 and resulting material properties”. Additive Manufacturing, Vol. 35, pp. 1-14.

Scholtes, B., 2000. “Residual stress analysis – a useful tool to assess the fatigue behavior of structural components”. Advances in X-ray analysis, Vol. 43, pp. 39-47.

Zinn, W., Scholtes, B., 2002. “Residual stress formation processes during welding and joining”. In: Totten, G., Howes, M., Inoue, T, 2002. “Handbook of residual stress and deformation of steel”. ASM International.

7. RESPONSIBILITY NOTICE

The authors are the only responsible for the printed material included in this paper.